national accelerator laboratory

TM-378
2526.000

PROPOSED CERENKOV TRIGGER COUNTER FOR BNL HYPERON BEAM

Arthur Roberts

June, 1972

Summary

In this note we investigate the feasibility of designing Cerenkov detectors for the present hyperon beam at BNL, capable of providing identifying triggers on the passage of a given hyperon. The counters are designed to accept the entire phase space occupied by the beam, and are constrained not to exceed in length one decay length of the hyperons. It appears to be readily possible to construct a simple and effective counter to trigger on omega-minus hyperons, distinguishing them from all other particles. However, it is pointed out that the probability of being able to observe omega-minus in the beam is extremely dependent on the omega-minus lifetime; a change by one standard deviation gives a factor of ten in decay in the beam. It is also possible, with some difficulty, to construct a counter to distinguish xi's from sigmas and other particles. A counter adaptable to both purposes can be constructed, but both separations cannot be carried out simultaneously in the existing beam; the mirror and photomultiplier layouts are different in the two cases.

PART I. OMEGA DETECTOR DESIGN

1. OMEGA LIFETIME AND SURVIVAL

The aim of observing omega-minus hyperons in the BNL hyperon beam in experiment 430 has now been pursued for some time, thus far without unequivocal success. Before designing an omega detector let us recall the strict limits on observability imposed by the fixed decay path, the momentum spectrum, and the omega-minus lifetime.

Lifetime - The Rosenfeld compilation (April, 1972) gives, for a total of 28 observed particles, the omega-minus lifetime:

$$c\tau = 3.9 \begin{matrix} + 1.2 \\ - 0.9 \end{matrix} \text{ cm.}$$

Taking into account the mass, this translates into the more convenient decay length per Gev/c momentum:

$$L_o = 2.33 \begin{matrix} + 0.79 \\ - 0.54 \end{matrix} \text{ cm/Gev/c.}$$

This is to be compared, e.g., with the cascade (minus) hyperon L_o = 3.77 cm/Gev/c. The minimum decay path attainable in the BNL beam is taken as 4.50 meters (177.3 inches). The fraction of particles surviving a decay path D is given by exp(-D/L), where $L = L_o p$ is the decay length; p is the momentum in Gev/c. This quantity is plotted in Fig. 1 against the reciprocal of L, for D = 4.5 meters.

Survival - Let us estimate the smallest survival fraction we think we can observe. At 21.5 Gev/c, the xi decay length is 81 cm, and the survival fraction is $4. \times 10^{-3}$. At nominal beam conditions, we see about 3 xi's per pulse at this momentum, or 6,000 per hour. Let us assume a yield of omegas 100 times

smaller.[1] Let us further assume an overall detection efficiency of 1/3 for omega detection, taking into account visible decay modes and spectrometer acceptance; this is probably optimistic. Then to observe one omega per hour we can allow another factor of 20 for decay. This gives a fraction surviving of $4 \times 10^{-3}/20 = 2 \times 10^{-4}$, corresponding to a decay length of 53.2 cm. The corresponding momenta for the mean and one-s.d. values of lifetime given above are 17.0, 22.8, and 29.7 Gev/c in descending lifetime order.

Thus, if we are lucky, and the lifetime is longer than the current best value, omegas may be observable to momenta below 20 Gev/c. If not, the lowest momentum at which an observable fraction survives may be above the kinematic limit, or so close as to produce a fatal contraction of the available phase space.

We continue on the supposition that omegas are observable in usable numbers, a supposition that existing, but thus far unanalyzed, data may be able to verify or disprove. In that case, the availability of a counter that can identify a beam hyperon before decay would make possible a whole range of physics now inaccessible, which is described elsewhere.[2]

With this caveat in mind, then, we proceed to describe the design of Cerenkov detector of the image-dissecting variety[3], accepting the beam emerging from the present BNL channel, and capable of distinguishing omegas from other beam particles.

2. BEAM PROPERTIES AND DETECTOR DESIGN

The design of a focusing Cerenkov detector depends critically on the properties of the particle beam. Some of the characteristics of the beam emerging from the magnetic channel are given in Figs. 2 and 3. The dimensions of the beam at the channel exit are 2.2 x 2.0 cm. Fig. 2 shows the angular spread of the beam, both horizontally and vertically. Fig. 3 is a plot of horizontal direction versus momentum, showing the dispersion of the channel and the finite angular resolution. It is this plot that primarily determines the Cerenkov detector design. The vertical spread of the beam is $\pm$ 3.25 mrad independent of momentum, as shown by Fig. 2. These data are from Monte Carlo calculations by J. Lach.

Since particles of a given momentum span a finite angular range, the centers of the Cerenkov rings they produce will span the same range.

The design procedure consists of determining, as a function of index of refraction, the size and location, in the focal plane, of the Cerenkov rings produced by particles of a given velocity and direction, within the limitations that the length of the counter should not much exceed one decay length, and that the cone angle be sufficient to produce an adequate number of photoelectrons at the photomultiplier cathodes. Fortunately these conditions can be met.

In order to obtain the narrowest spread of Cerenkov images for the desired particles, the index of refraction should be so chosen that the horizontal dispersion of the beam (which at 23 Gev/c is about 3.8 mrad/Gev) is just equal to

the rate of change of the Cerenkov cone angle with velocity. Thus, as the momentum increases, the center of the Cerenkov circle moves over just the same amount that the angular radius of the ring image increases, producing a series of rings all tangent at the same point. This condition can be approximately met over a small range of index of refraction, allowing some choice of this variable.

The residual width is then due to the angular span, at its widest point, of the distribution of Fig. 3. Fig. 4a is a plot showing the location of the intersections with the horizontal axis of Cerenkov ring images of omegas and xi's in the momentum range 19.2 - 23.7 Gev/c, with the angular distribution of Fig. 3, for an index of refraction 1.0060. The sign of the momentum dispersion is such as to cancel the separation of the different momenta on the left side and enhance it on the right side. On the left side the resolution is adequate to identify omegas, but not to separate sigmas and xi's. Relativistic particles, labelled pions (which includes muons and electrons), can be separated from the hyperons. On the right-hand side only a partial separation is possible. Figs. 4b and 4c show the possibility of changing the momentum acceptance range by changing the index of refraction. The separation remains good over the range 17-27 Gev/c.

Defocusing effects - In addition to the width due to angular spread and momentum dispersion, the Cerenkov images are blurred by chromatic dispersion in the Cerenkov medium. Each image becomes, in effect, a zone about 2% wide (using wavelengths down to 300 nm). At a mean angle of 75 mrad this amounts to

1.5 mrad to be added to the outer edge of each mirror segment. In addition, each circle must be thought of as being smeared out by $\pm$ 3.5 mrad in the direction perpendicular to the dispersion axis; this is due to the vertical divergence of the particles. This affects the mirror boundaries at the points farthest from the axis.

The complete set of circles for the respective particles is given in Figs. 5a to 5d. The dotted curves show extensions required by widening the momentum range covered, as shown in Figs. 4b and 4c.

3. MIRROR DESIGN

The final mirror design proposed is shown in Fig. 6. This design has the following features, as may be verified by superposing the images of Figs. 5 and 6.

1. Three mirror segments are provided which only omegas can illuminate (1, 1a and 2). Numbers 1 and 1a cover the entire momentum spectrum, 2 only the lower half. The remainder of the momentum spectrum is registered on number 3.

   An omega trigger is therefore defined as 1 · 1a · (2 + 3). All other segments are placed in anti-coincidence. Subdivision into 4 rather than 3 segments is possible; it reduces the efficiency for the slowest omegas below 80%; requiring 5 segments would drop the efficiency to 56%.

2. An impure, but "enhanced" xi trigger, free of pions but not of sigmas, can be simultaneously provided by a similar arrangement 4 · 4a · (3 + 5). Alterna-

tively, by increasing the outer radii of these mirrors somewhat, a (sigma + xi) trigger can be provided, free of pions and omegas, but without xi enhancement.

3. An anticoincidence counter for pions, number 6, is available if desired; it may perhaps be useful also in reducing stray muon background. If it is not desired, the overall diameter of the dissecting mirror assembly can be somewhat reduced.

Table 1 shows the mirror and trigger logic.

4. INTENSITIES

A calculation of the number of photoelectrons to be expected is shown in Table 2. The number varies from about 10.1 to 17.6 for omegas; it is higher for xi's. These numbers determine how much the circles can be subdivided among several coincident photomultipliers. The larger the number of photomultipliers the better the identification and background rejection; but too large a number will result in a drop in detection efficiency. The efficiencies shown are for the division and logic of Fig. 6 and Table 1.

Table 1 - Logic Tables for Mirror Segments

Segment	Particles Seen
1, 1a	Ω
2	Ω
3	Ω, Ξ, Σ
4, 4a	Ξ, Σ, (π^-)
5	Ξ, Σ, π
6	Σ, π
7	background

Trigger Logic

(counters not in trigger are in anticoincidence)

Ω	$1 \cdot 1a \cdot (2 + 3)$
Ξ, Σ	$4 \cdot 4a \cdot (3 + 5)$
π	6

Table 2 - Intensities and Ω Detector Efficiencies

Most probable number of photoelectrons is calculated from $N = 50\ \ell \sin^2 \theta$, $\ell = 50$ cm. (Note - index of refraction is not the same at all momenta.)

P	θ (mrad)	N	N/4	$1-e^{-N/4}$	Detection Efficiency
17.35	63.7	10.1	2.55	.914	0.84
19.2	66.5	11.05	2.76	.937	0.88
21.45	77.1	14.8	3.70	.975	0.95
23.7	83.9	17.6	4.40	.988	0.976
24.5	77.1	14.8	3.70	.975	0.95
27.1	82.5	17.0	4.25	.985	0.97

5. COUNTER DESIGN

Fig. 7 shows a drawing of a Cerenkov detector embodying the designs implied above. The radiator length has been kept down to 50 cm. The Cerenkov images are formed at a focal length of 110 cm with the aid of a 90° reflection. The 45° reflecting mirror must very thin (i.e., a pellicle) to avoid interactions in the beam region, and the spherical (or parabolic) focusing mirror, which must be about 15 cm in diameter, should be thin in the central region through which the beam passes; a hole to pass the beam would significantly decrease the effective radiator length.

The focal length is chosen to be 100 cm to leave sufficient room for the photomultipliers that ring the light beam incident on the dissecting mirrors in the Cerenkov image plane. These

mirrors must be of short focal length for the same reason; the design of Fig. 7 uses a focal length of 30 cm.

6. MECHANICAL DESIGN FEATURES

In order to obtain the required index of refraction, 1.0060 or thereabouts, freon at about 100 psia is required. Since this pressure is too high for conventional photo-multiplier tube envelopes, a pressure-tight window is required in the optical path. In Fig. 7 this is shown on the top of the counter just about the 45^{o} mirror, where the optical diameter is smallest. This window needs to be about 8" in diameter. It should be uv-transmitting, preferably quartz or fused silica. Quartz discs in this size are available; uv-transmitting lucite may be practical also.

PART II. CASCADE HYPERON DETECTOR DESIGN

The problem of obtaining a reasonably pure xi trigger is worth considering, since xi decays and inter-actions are far from being well understood, not much data are available. The already established abundance of xi's (3 per pulse) guarantees the possibility of a wide vareity of studies; these will be treated elsewhere.

In order to separate the xi from the sigma, the mas difference now being only 10% rather than the 26% xi-omega mass difference, it is essential to achieve the narrowest possible

xi tangency band, by cancelling the dispersion as accurately as possible. For xi's, unfortunately this happens at considerably lower indices of refraction and cone angles (unless we are willing to decrease the momentum range considerably.) The xi yield is at a maximum in the BNL beam at 21.5 Gev/c. Fig. 8a shows the best sigma-xi separation possible; it occurs for n = 1.0031, and a cone angle around 39 mrad for the 19.2 Gev/c xi's. At this cone angle we get only 3.75 photoelectrons in a 50-cm long radiator, so that detection efficiency for a threefold coincidence drops to 36%. A slightly better compromise is shown in Fig. 8b, for the index 1.0035, a minimum cone angle of 48 mrad, and a threefold coincidence efficiency of 62%, rising to 82% at 21.45 Gev/c. There is a slight overlap at this index of sigmas into the xi mirror; the high-energy sigmas that overlap are cancelled out on the opposite side of the mirror array, however.

To improve the marginal detection efficiency the length of the counter could be increased; going from 50 cm to 65 cm would raise the detection efficiency at 19.2 Gev/c from 62% to 76.5%. An equivalent improvement in photocathode efficiency by tube selection would have the same effect (i.e., raising the constant in the equation for the number of photoelectrons from 50 to 65.)

If we assume that such phototube selection is possible, then we can design the mirror array for xi-sigma separation. Fig. 9 shows the particle images for xi, sigma, and pi, as

well as proposed mirror boundaries. Table 3 shows the counter logic and triggering logic for this mirror layout. Practically complete separation should be possible, with pure xi and sigma triggers of good efficiency

Table 3 - Counter Logic for Σ-Ξ Separation

Segment	Particles
1, 2	Ξ, sigmas near 23.7 Gev/c
3	Ξ
4, 5	all Σ, including those at 23.7 Gev/c
6	Ξ, Σ (no sigmas that strike 1 or 2)
7	Ξ 23.7, all Σ, π
8	π
9	background, junk

Trigger Logic

Ξ	$1 \cdot 2 \cdot (3 + 6 + 7)$ Note: Sigmas of 23 · 7 Gev/c are detected with efficiency 0.017
Σ	$(4 \cdot 5) \cdot (6 + 7)$
π	8

Figure Captions

Fig. 1 The fraction of incident particles that survive a decay path of 4.50 meters, as a function of the reciprocal of the decay length in meters.

Fig. 2 Monte Carlo distribution for the vertical and horizontal angular spread of the hyperon beam at the channel exit. They are respectively about $\pm$ 3.6 mrad, $\pm$ 11.0 mrad.

Fig. 3 The horizontal spread of the beam at the channel exit as a function of the particle momentum. The channel is tuned to cover the range from about 19 to 26 Gev/c; other momenta scale proportionally. The angular spread at any one momentum determines the best mass or velocity resolution possible; the wider the spread, the poorer the resolution.

Fig. 4 The angular range of the intersections with the horizontal axis of the Cerenkov rings produced by the distribution of Fig. 3. The distribution is sampled at three momenta, and the angular range covered is shown for both the left side, where the momentum dispersion is a minimum, and the right side, where it is maximum. a) This case, for n = 1.0060, and the momentum range 19.2 - 23.7 Gev/c, shows the best cancellation of momentum dispersion for omegas. The corresponding xi and sigma intersections are shown. b) The momentum range is now 21.7 to 27.2 Gev/c, and the index has been readjusted to n = 1.00529 to bring the distribution back as closely as possible to the original angular range. c) The same, with n =

1.00668, for the momentum range 17.2 to 21.5 Gev/c. For all these cases, the omega-xi separation remains adequate; the xi range must be extended inward to cover the lower momenta.

Fig. 5 These figures show the range of Cerenkov rings for the constants of Fig. 4a above. Figs. 5a, 5b, 5c and 5d are respectively for omega, xi, and sigma hyperons, and pions. The dotted lines indicate the extensions necessitated by the extensions of momentum range of cases 4b and 4c.

Fig. 6 Proposed segmented mirror design. If the pion anticoincidence feature is not required, mirror number 6 can be omitted or terminated at a smaller radius. Nine mirror segments are used, requiring eight phototubes. The radii shown are in mrad; in the design of Fig. 7, the scale is 1 mrad = 1.1 mm.

Fig. 7 Sketch of the proposed design of the counter. The radiator length is 50 cm; the Cerenkov mirror is 15 cm diameter, focal length 110 cm. The operator pressure is about 100 psia of freon-12. A quartz or silica window above the 45^{o} mirror separates the pressurized volume from the dissecting mirror and phototubes, which are therefore detachable and accessible without disturbing the radiator volume.

Fig. 8 Constants for separating xi from sigma, in the momentum range 19.2 - 23.7 Gev/c. a) Optimum separation, with n = 1.0031, best cancellation of xi momentum dispersion. b) n = 1.0035; separation of xi from sigma no longer

complete, but radius of circles appreciably larger, giving more nearly adequate intensities.

Fig. 9 A superposition of the Cerenkov circles for xi's, sigmas, and pions; the proposed mirror boundaries are shown in dotted lines.

References

1. The basis for this estimate is the following. The ratio of xi to sigma production by protons on a heavy target at BNL is about 1:30. These two particles represent strangeness changes of one and two units respectively. In addition, Mr. P. Schultz has kindly communicated to us the results of a University of Illinois bubble-chamber experiment on hyperon production by 5.5 Gev/c K^- in hydrogen. He finds the total production cross-sections of omegas to be 4 μb, of xi's 144 μb, a ratio of 1:35 (this is based on only three omega events). The strangeness change is the same as in the BNL case. If we assume this to be the governing factor, then the next unit of strangeness should give the same cross-section reduction. The factor of 100 is taken on the pessimistic side.
2. J. Marx, in preparation.
3. A. Roberts, Nucl. Instr. and Methods, 99, (1972), p. 589.

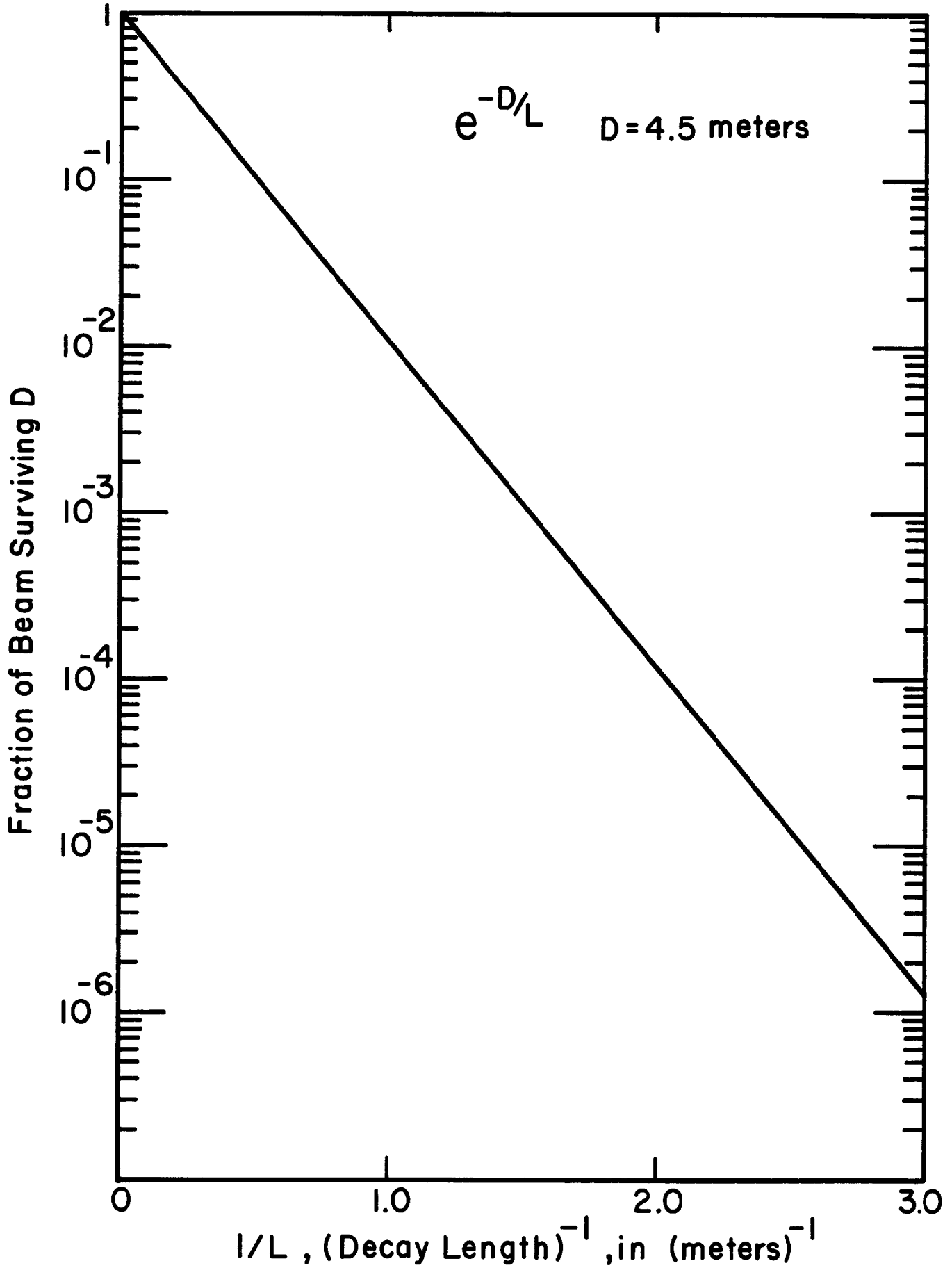
$e^{-D/L}$
D = 4.5 meters
Fraction of Beam Surviving D
1
10^{-1}
10^{-2}
10^{-3}
10^{-4}
10^{-5}
10^{-6}
0
1.0
2.0
3.0
1/L , (Decay Length)$^{-1}$, in (meters)$^{-1}$

Fig. 1

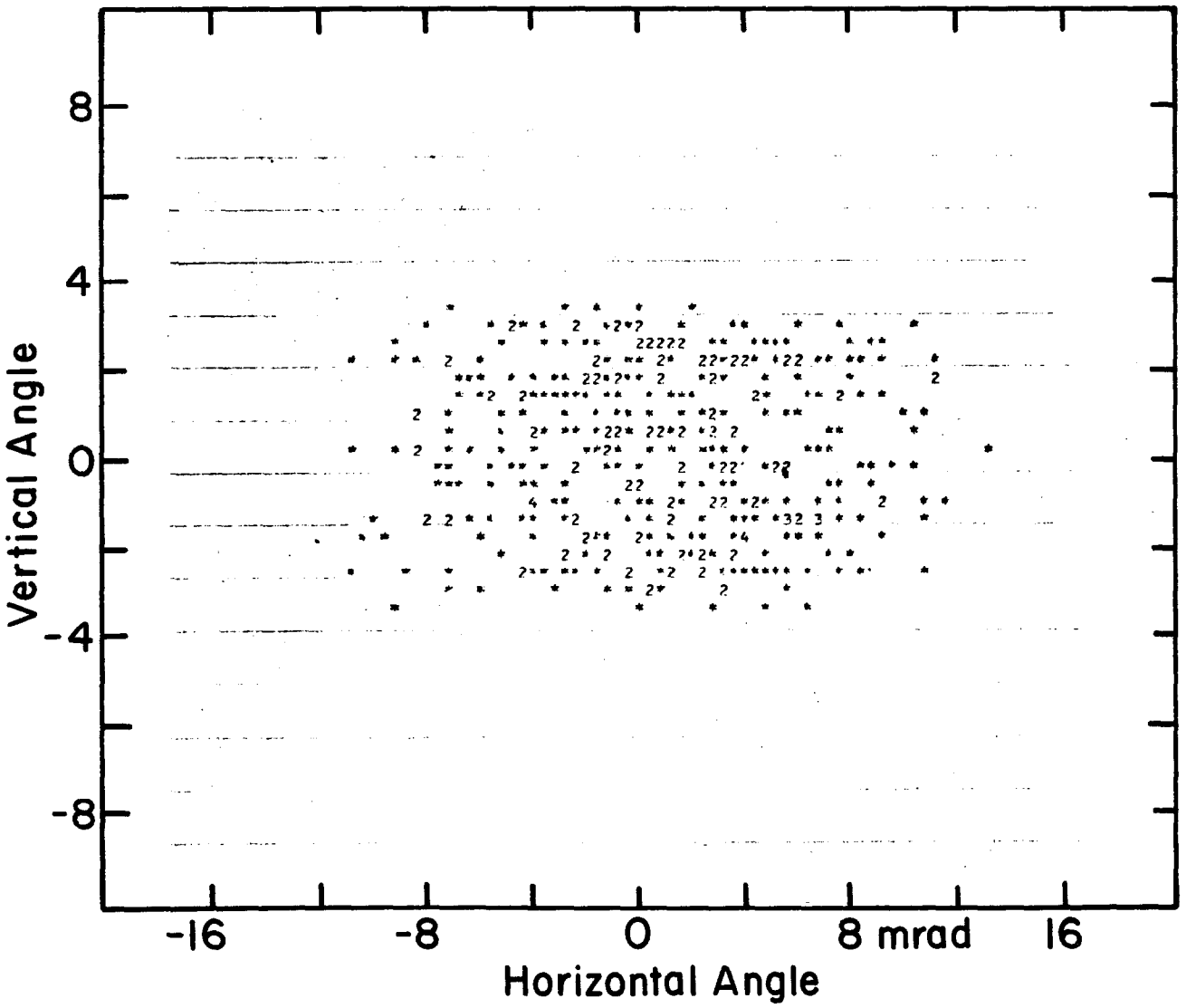

Fig. 2

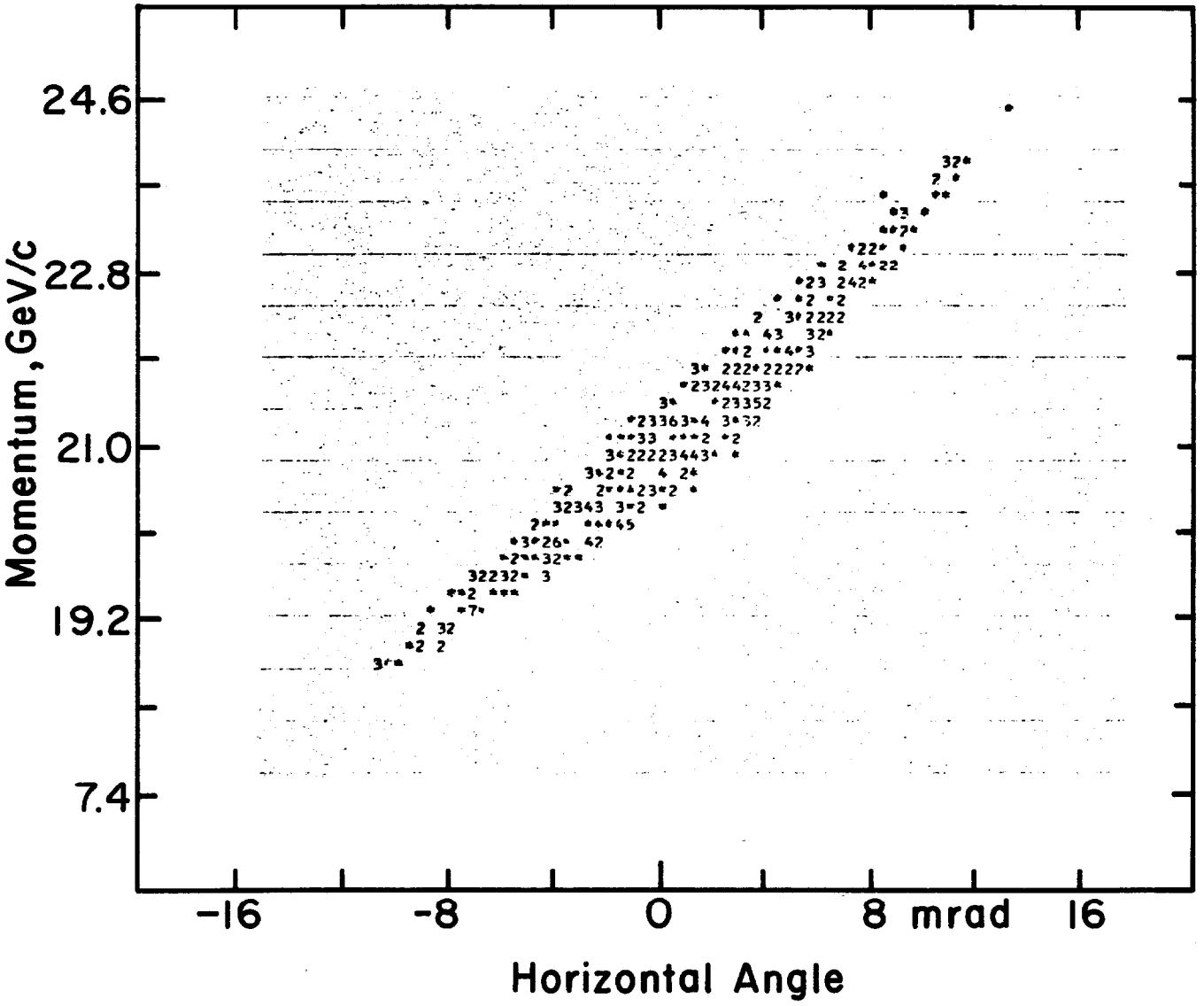
24.6
22.8
21.0
19.2
7.4
Momentum, GeV/c
-16
-8
0
8 mrad
16
Horizontal Angle

Fig. 3

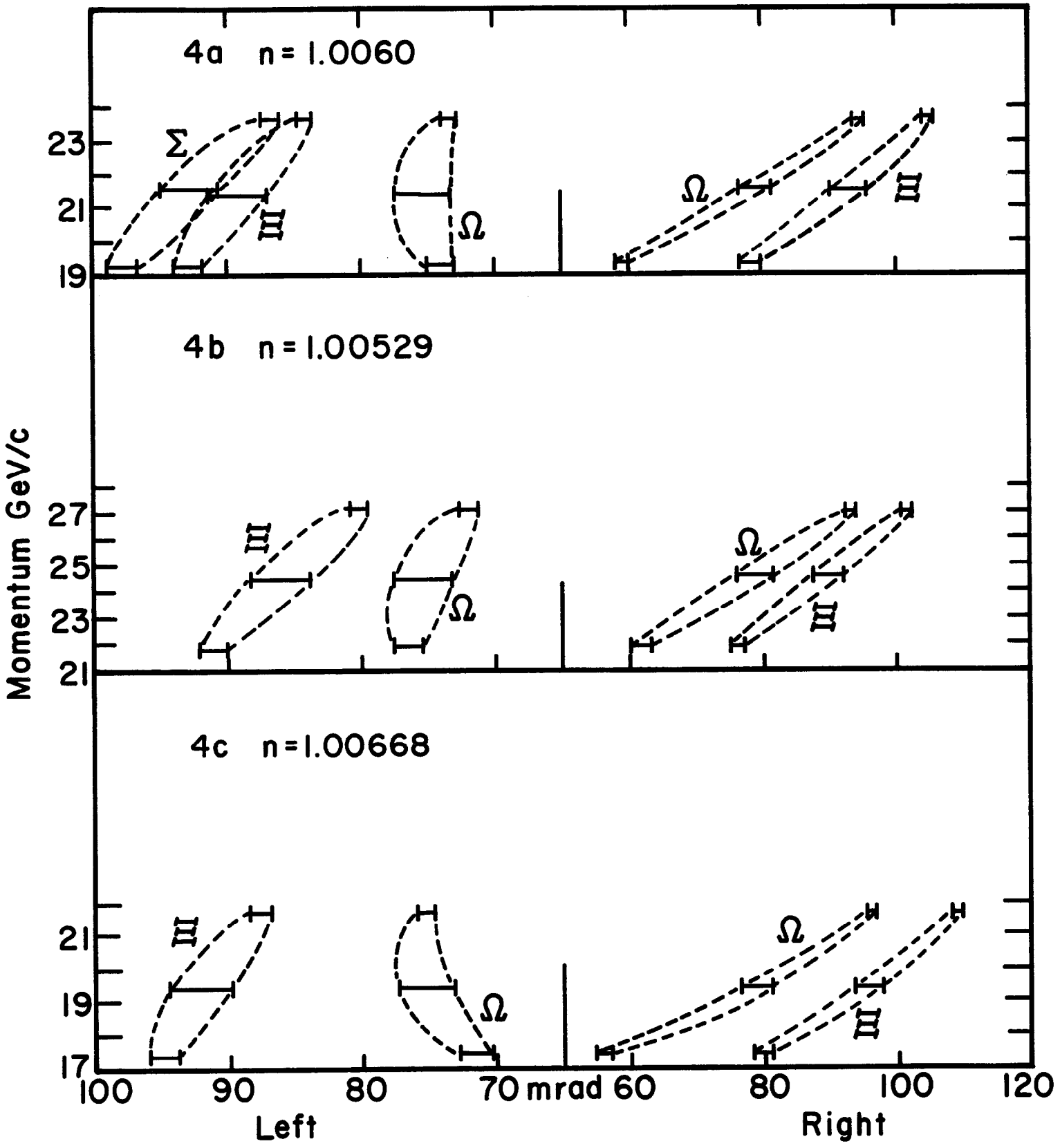
4a n = 1.0060
4b n = 1.00529
4c n = 1.00668
Momentum GeV/c
23
21
19
27
25
23
21
21
19
17
Σ
Ξ
Ω
Ω
Ξ
Ξ
Ω
Ω
Ξ
Ξ
Ω
Ω
Ξ
100
90
80
70 mrad 60
80
100
120
Left
Right

Fig. 4

Fig. 5(a)

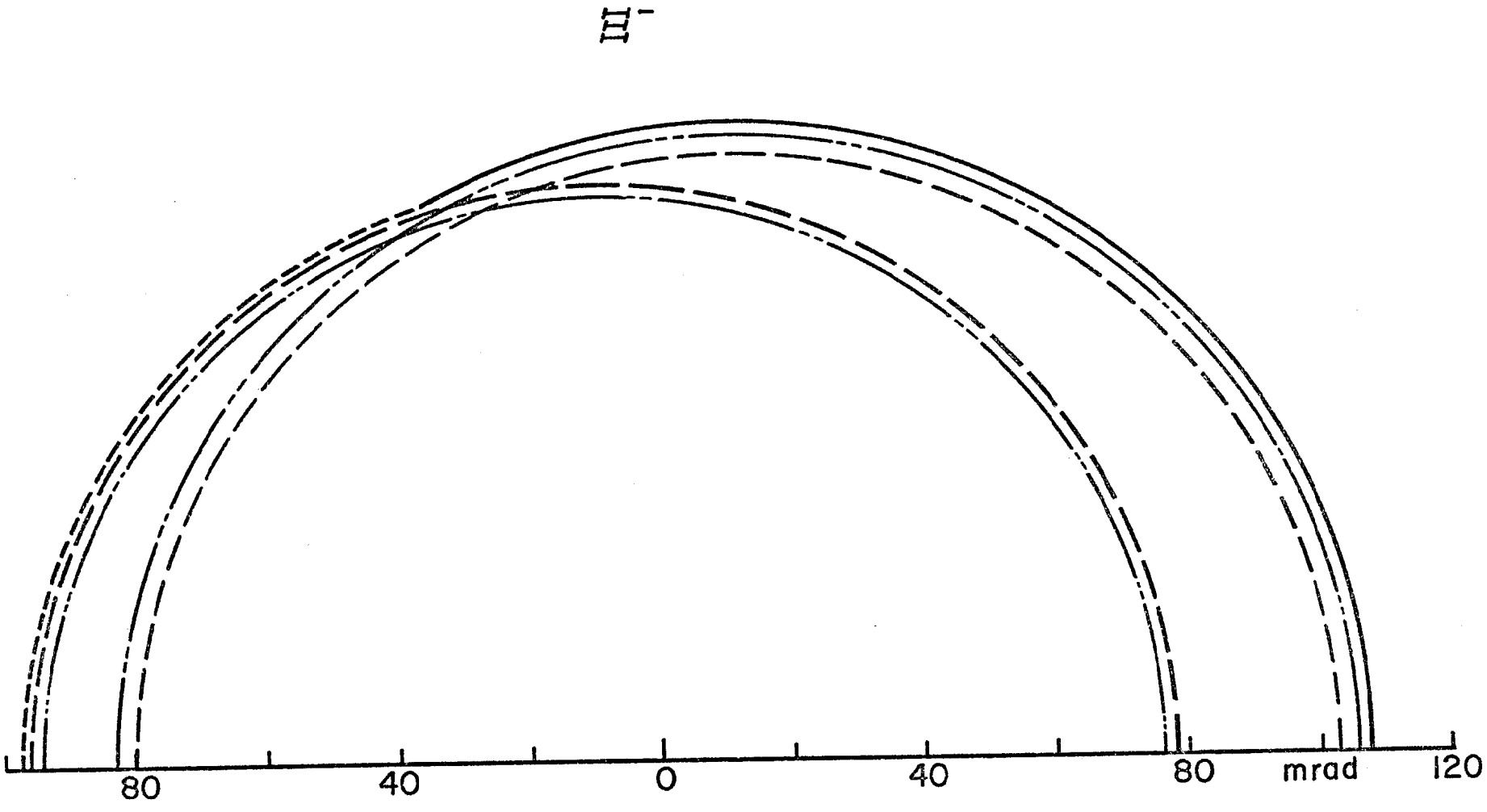

Fig. 5(b)

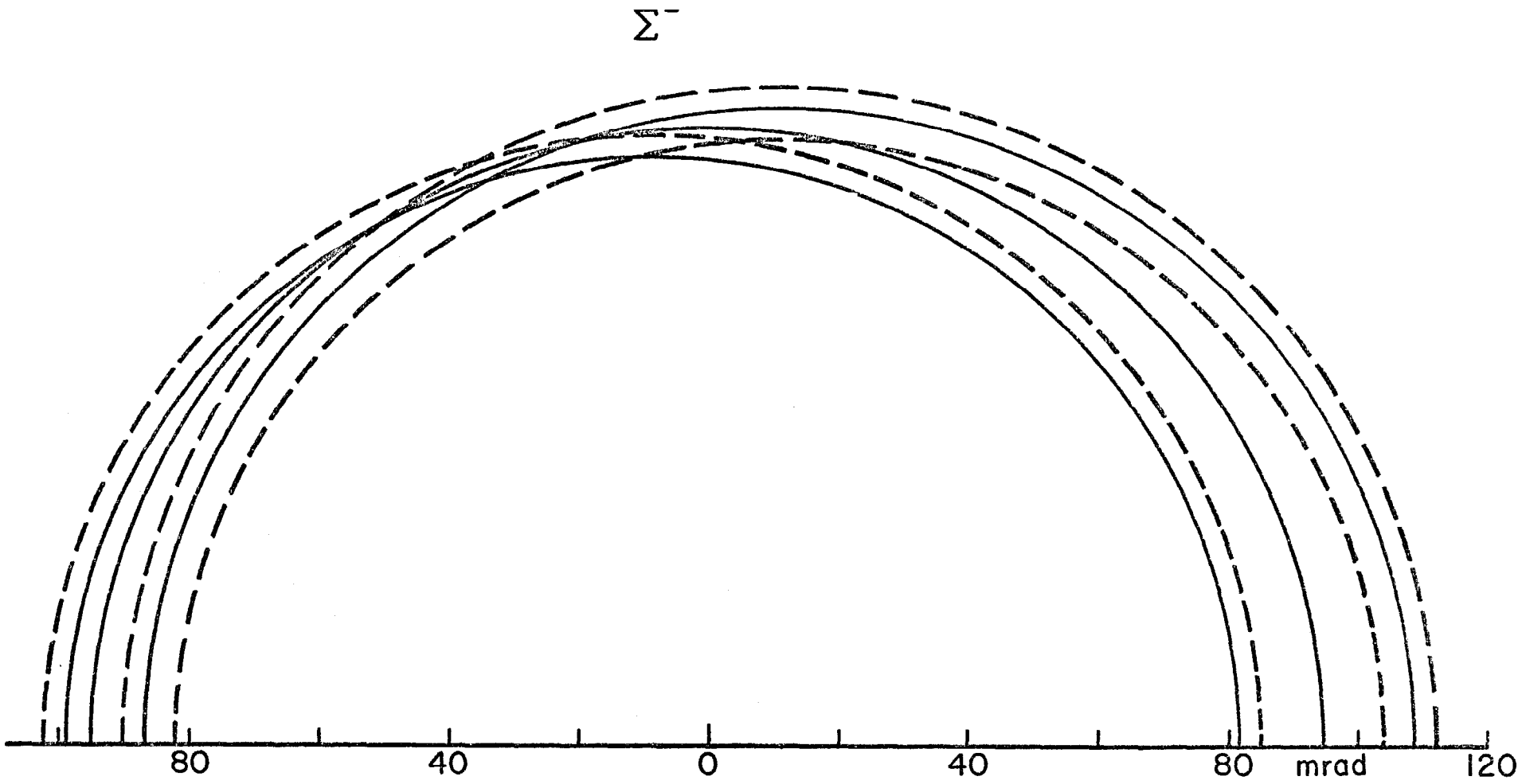

Fig. 5(c)

Fig. 5(d)

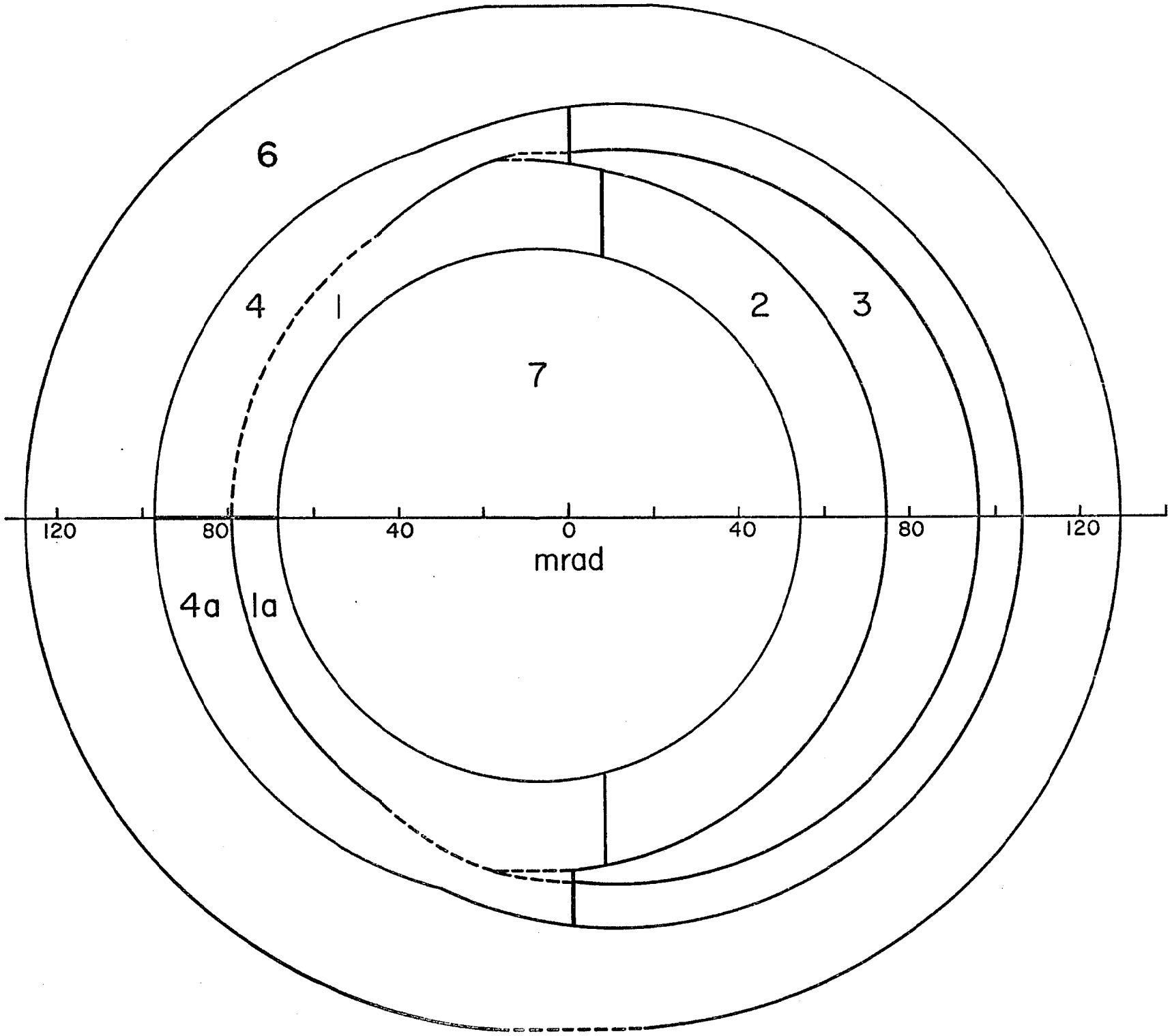

Fig. 6

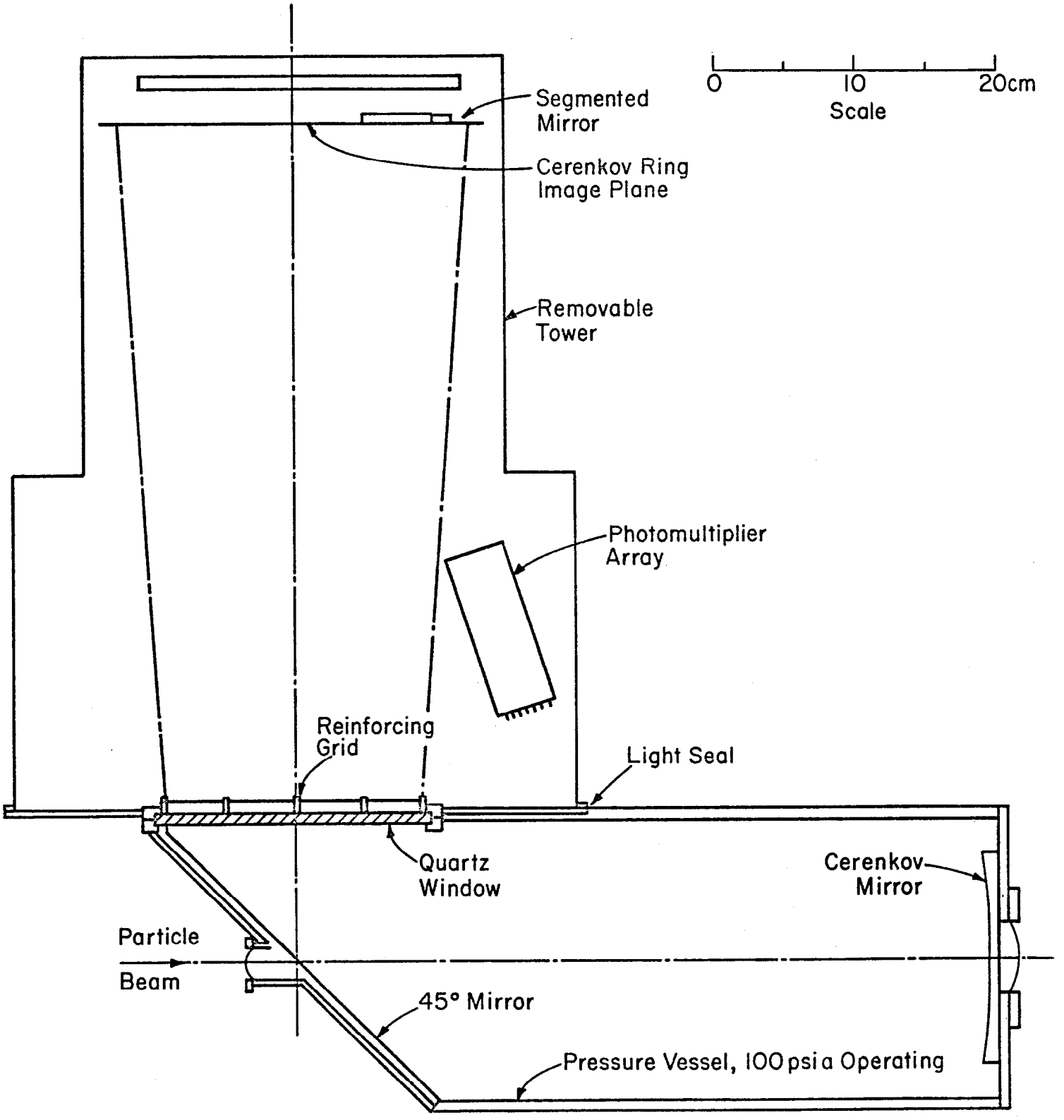
0
10
20cm
Scale
Segmented Mirror
Cerenkov Ring Image Plane
Removable Tower
Photomultiplier Array
Reinforcing Grid
Light Seal
Quartz Window
Cerenkov Mirror
Particle Beam
45° Mirror
Pressure Vessel, 100 psia Operating

Fig. 7

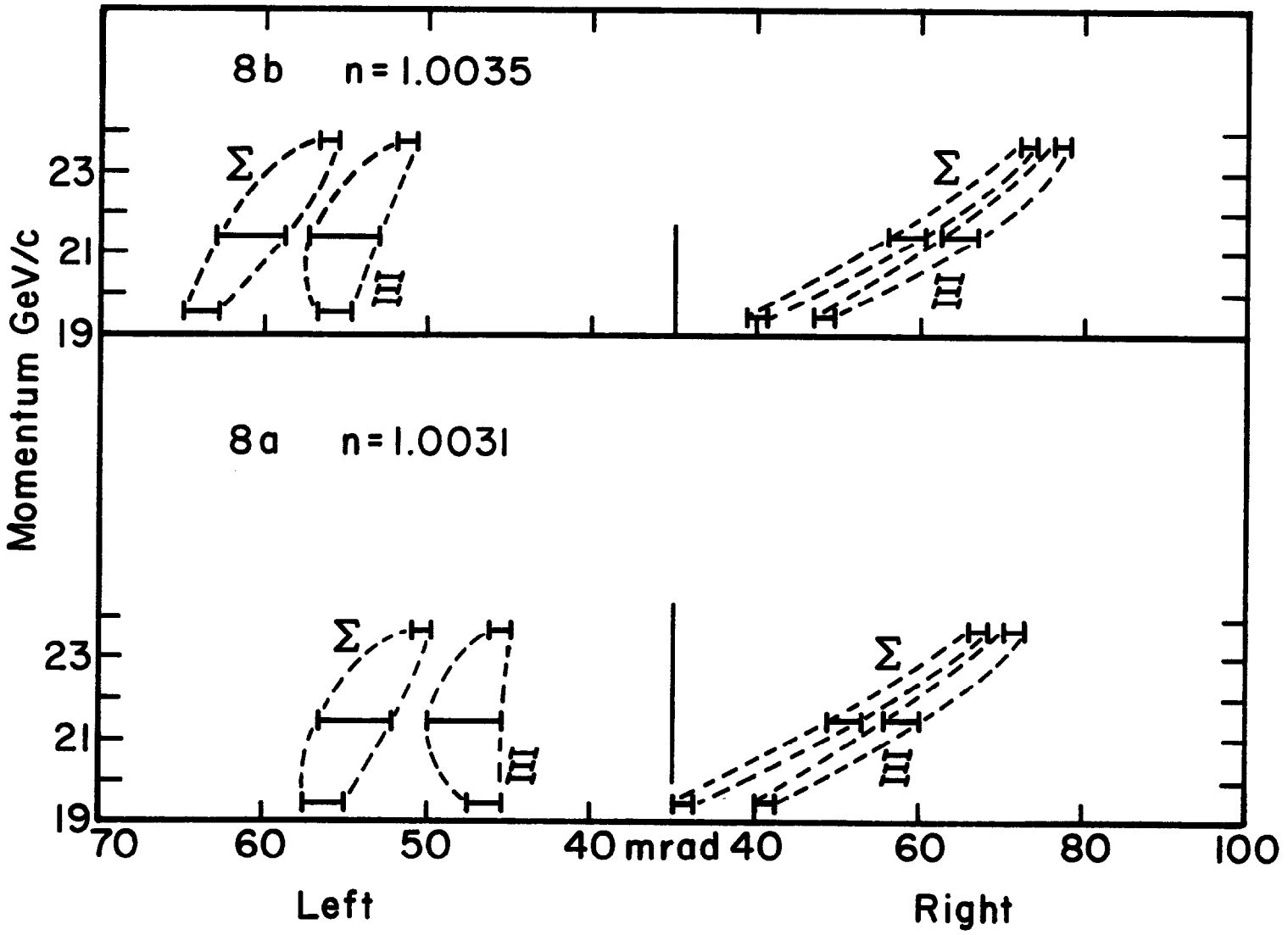
8b n=1.0035
8a n=1.0031
Momentum GeV/c
23
21
19
Σ
Ξ
70
60
50
40 mrad 40
60
80
100
Left
Right

Fig. 8

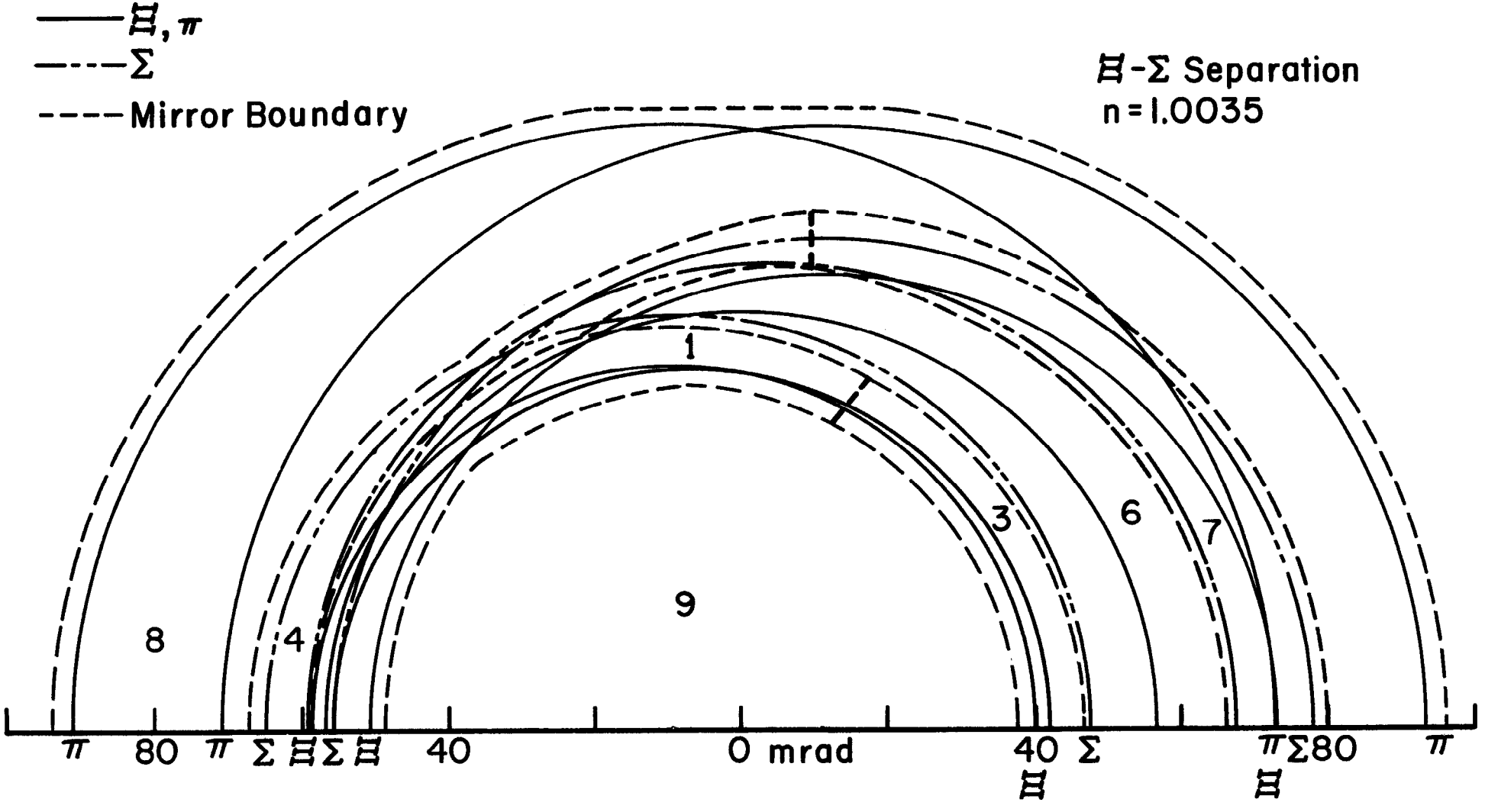
Ξ, π
Σ
Mirror Boundary
Ξ-Σ Separation
n=1.0035
1
3
6
7
9
8
4
π 80 π Σ Ξ Σ Ξ 40 0 mrad 40 Σ 80 π
Ξ
Ξ

Fig. 9